ChemComm

Bisulfate as a Redox-active Ligand in Vanadium-based Electrocatalysis for CH_4 Functionalization

Journal:	*ChemComm*
Manuscript ID	CC-COM-11-2021-006596.R1
Article Type:	Communication

COMMUNICATION

Bisulfate as a Redox-active Ligand in Vanadium-based Electrocatalysis for CH_4 Functionalization†

Received 00th January 20xx,
Accepted 00th January 20xx

DOI: 10.1039/x0xx00000x

Danlei Xiang,‡[a] Sheng-Chih Lin,‡[b] Jiao Deng,[a] Hao Ming Chen*[b] and Chong Liu*[a,c]

The roles of the unforgiving H_2SO_4 solvent in CH_4 activation with molecular catalysts have not been experimentally well-illustrated despite computational predictions. Here we provide experimental evidence that metal-bound bisulfate ligand introduced by H_2SO_4 solvent is redox-active in vanadium-based electrocatalytic CH_4 activation that we discovered recently. Replacing one of the two terminal bisulfate ligands with redox-inert dihydrogen phosphate in the electrochemical pre-catalyst vanadium(V)-oxo dimer completely quenches its activity towards CH_4, which may inspire environmentally benign catalysis with minimal use of H_2SO_4.

The abundance of methane (CH_4) welcomes sustainable methods of converting CH_4 into fuels or commodity chemicals such as methanol (CH_3OH) at low temperatures.[1] Since the existing two-step industrial route of CH_4-to-CH_3OH conversion is capital-intensive and operates under high temperatures and pressures,[2] direct activation and two-electron oxidation of CH_4 with molecular transition-metal-based catalysts offers an attractive alternative. In those systems, concentrated sulfuric acid (98% H_2SO_4) or even oleum ($H_2SO_4{\cdot}xSO_3$)[1c, 3] are frequently applied as the solvent in homogenous[4] and electrochemical catalysis[5] in order to mitigate undesirable further oxidation, thanks to the formation of oxidatively stable methyl bisulfate (CH_3OSO_3H),[6] a precursor of CH_3OH, as the product of two-electron oxidation of CH_4. Yet it is proposed computationally that there are additional roles of H_2SO_4 solvent in the critical step of homogeneous Au^{III}, Pd^{II}, Hg^{II}, Sb^{V}-based CH_4 activation[7]—metal-bound bisulfate ligand ($-OSO_3H$) undergoes an intramolecular abstraction of proton from CH_4 concurrent with the formation of metal–CH_3 bond (Fig. S1). Other roles of the bisulfate ligand are suggested in electrocatalytic CH_4 activation in H_2SO_4. We previously reported room-temperature electrochemical CH_4 functionalization into CH_3OSO_3H in 98% H_2SO_4 with molecular catalyst vanadium(V)-oxo dimer $V_2^{V,V}$ (**1** in Fig. 1).[5c] Kinetics of the electrocatalysis suggests that preceding CH_4 activation there exists a turnover-limiting electrochemical oxidation of d^0 $V_2^{V,V}$ into a CH_4-reactive cation radical $V_2^{V,V\bullet+}$, which is computationally predicted to be an oxygen radical mostly localized on the monodentate bisulfate ligand (Fig. 1a). Moreover, it is computationally suggested that CH_4 activation on an electrochemically generated $Pd_2^{III,III}$ dimer is initiated on the metal-bound bisulfate via an H-atom abstraction process (Fig. S1),[8] which similarly hints a redox-active bisulfate ligand with an O atom radical. Such mechanistic insights suggest that the bisulfate ligand hence the H_2SO_4 solvent is critical towards the observed activities in both homogenous and electrochemically catalytic systems. However, experimental evidence remains elusive. A deeper understanding about the

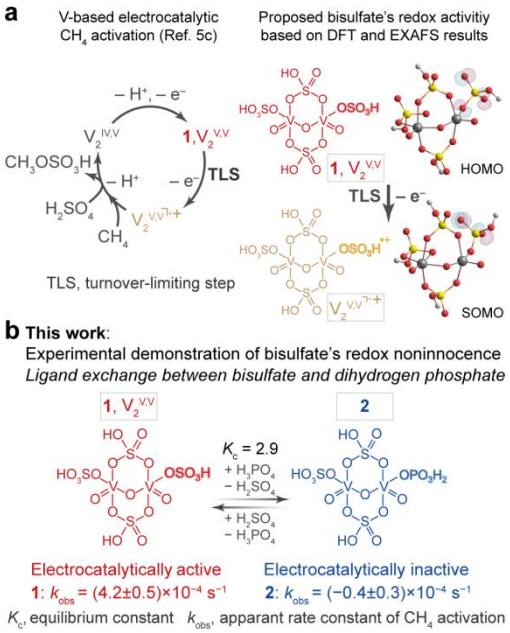

Fig. 1 a, The proposed mechanism of CH_4 functionalization initiated by the electrochemically generated cation radical ($V_2^{V,V\bullet+}$) from a vanadium (V)-oxo dimer (**1**, $V_2^{V,V}$, based on DFT and EXAFS results).[5c] **b**, Mono-substitution of bisulfate with dihydrogen phosphate ligand leads to electrocatalytically inactive **2** in H_2SO_4-H_3PO_4 mixed solvent.

[a] *Department of Chemistry and Biochemistry, University of California Los Angeles, Los Angeles, California 90095, United States. E-mail: chongliu@chem.ucla.edu*
[b] *Department of Chemistry, National Taiwan University, Taipei 10617, Taiwan. E-mail: haomingchen@ntu.edu.tw*
[c] *California NanoSystems Institute, University of California Los Angeles, Los Angeles, California 90095, United States.*
‡ Danlei Xiang and Sheng-Chih Lin have equally contributed to this work.
† Electronic Supplementary Information (ESI) available: Full experimental details, data analysis and additional figures. See DOI: 10.1039/x0xx00000x

H_2SO_4 and bisulfate ligand's role in the CH_4-activating catalytic cycle will help us to design environmentally benign catalytic systems with minimal use of 98% H_2SO_4 while yielding CH_3OH or its equivalent without excessive oxidation.

Here we seek to experimentally validate the redox noninnocence of the bisulfate ligand in the context of searching for an alternative electrolyte other than the unforgiving H_2SO_4. Because the formal oxidation state of the vanadium(V) metal centers cannot be further increased, the electrocatalytic CH_4 activation based on $V_2^{V,V}$ pre-catalyst[5c] (Fig. 1) is selected as a model system devoid of the potential interference from metal-based redox changes. We hypothesize that substituting the monodentate bisulfate ligand with a more redox-inert dihydrogen phosphate moiety ($-OPO_3H_2$)[9], by partly replacing H_2SO_4 solvent with H_3PO_4, is an effective perturbation of the catalytic center and a venue to probe the role of bisulfate ligand (Fig. 1b).

We observed a chemical equilibrium between $V_2^{V,V}$ (**1**) and the variant mono-substituted by a dihydrogen phosphate ligand (**2**) in solvent mixtures of H_3PO_4 and H_2SO_4. UV-Vis spectrometry was conducted when V_2O_5 was dissolved in H_3PO_4-H_2SO_4 electrolytes of different molar concentration ratios c_{H3PO4}/c_{H2SO4} (Fig. 2a, ESI†). A symmetric bimodal distribution of absorption peaks with an isosbestic point at 309 nm was observed when the total vanadium concentration C_V = 0.4 mM (Fig. 2a). In 98% H_2SO_4 (i.e. c_{H3PO4}/c_{H2SO4} = 0/18.0), the strong absorption peak at λ_{max} = 329 nm is assigned to the ligand-to-metal charge-transfer (LMCT) band of **1**.[5c, 10] With the introduction of H_3PO_4 solvent hence the dihydrogen phosphate ligand, an isosbestic point in Fig. 2a suggests that only one new species **2** at λ_{max} = 291 nm formed at the expense of **1**. The blue-shifted LMCT band in **2** indicates that **2** contains a larger energy gap of LMCT and a less oxidatively accessible ligand-based molecular orbitals given the same d^0 vanadium(V) metal centers in **1** and **2**.[11] Such a stabilization of ligand-like molecular orbitals is consistent with the presumed ligand substitution by redox-inert dihydrogen phosphate.[12] Taking advantage of the isosbestic point,[13] we established a mathematical model to determine the equilibrium constant between **1** and **2** (K_c) and the number of bisulfate ligand substituted by dihydrogen phosphate (n),

$$\mathbf{1} + n\ H_3PO_4 \leftrightarrow \mathbf{2} + n\ H_2SO_4 \qquad K_c = \frac{[\mathbf{2}]^1 c_{H2SO4}{}^n}{[\mathbf{1}]^1 c_{H3PO4}{}^n} \quad (1)$$

$$log_{10}\left(\frac{[\mathbf{1}]}{[\mathbf{2}]}\right) = -\ log_{10}(K_c) + n\ log_{10}\left(\frac{c_{H2SO4}}{c_{H3PO4}}\right) \quad (2)$$

In a mixed solvent of a specific c_{H3PO4}/c_{H2SO4} value, the absorbances at 329 nm and 291 nm depend on the concentrations of **1** and **2** ([**1**] and [**2**], respectively), as well as their molar extinction coefficients at 329 nm and 291 nm. Analysis of Fig. 2a yields the values of [**1**] and [**2**] at different values of c_{H3PO4}/c_{H2SO4} (Fig. 2b and Table S1, ESI†). When c_{H3PO4}/c_{H2SO4} > 4.7/13.5, the biphosphate-substituted **2** becomes the predominant species. Following eqn (2), plotting $\log_{10}([\mathbf{1}]/[\mathbf{2}])$ against $\log_{10}(c_{H2SO4}/c_{H3PO4})$ yields a linear relationship (Fig. 2c) with its slope and y-intercept corresponding to n and $-\log_{10}(K_c)$, respectively. As n = 1.18 and K_c = 2.9 from Fig. 2c (ESI†), an equilibrated mono-substitution of bisulfate ligand with dihydrogen phosphate between **1** and **2** is established.

X-ray absorption spectroscopy suggests that the mono-substitution occurs on the terminal bisulfate ligand. Two vanadium solutions with c_{H3PO4}/c_{H2SO4} = 3.5/14.6 and 7.0/11.3 were measured with C_V = 10 mM. In the results of X-ray absorption near-edge structure (XANES) spectra for the vanadium atoms, the sample of c_{H3PO4}/c_{H2SO4} = 7.0/11.3 displayed a slight higher formal oxidation state of vanadium center than the one of c_{H3PO4}/c_{H2SO4} = 3.5/14.6, which is consistent with the substitution of a less oxidatively accessible $-OPO_3H_2$ that shifts the rising-edge and edge maxima of vanadium atoms to higher energy regions (Fig. S2a and S2b). Fig. 2d shows the extended X-ray absorption fine structure (EXAFS) spectra for samples with c_{H3PO4}/c_{H2SO4} = 3.5/14.6 (yellow trace) and 7.0/11.3 (blue trace), mixtures of **1** and **2** with molar ratios quantifiable from Fig. 2b. Fig. 2e shows the average fitting results from EXAFS based on the coexistence of **1** and **2**. In the first coordination shell near the metal, there are five V-bound O atoms with three different V–O bond lengths (Fig. 2d, blue area). The second coordination shell (Fig. 2d, > 2.0 Å, green area) includes the other V atom in the dimer structure and two S atoms from two bridging bisulfates; more importantly, there are S or P atoms less than one equivalent from the non-bridging $-OSO_3H$ or $-OPO_3H_2$ moiety (V–S and V–P, respectively, with a subscript "a" in Fig. 2e) and the averaged coordination numbers of the terminal $-OSO_3H$ and $-OPO_3H_2$ add up to one equivalent in both two samples. This suggests that the mono-substitution observed from UV-Vis spectrometry in Fig. 2a corresponds to the replacement of one non-bridging bisulfate ligand with dihydrogen phosphate. On average, the ratios of coordination numbers of the non-bridging terminal $-OSO_3H$ and $-OPO_3H_2$ ligand ($C.N._{V-S}/C.N._{V-P}$) from EXAFS are quite comparable with the expected ratios obtained from UV-Vis spectrometry in Fig. 2b (Table S2), corroborating the mono-substitution on the terminal bisulfate ligand (Fig. 1b) and offering a suitable

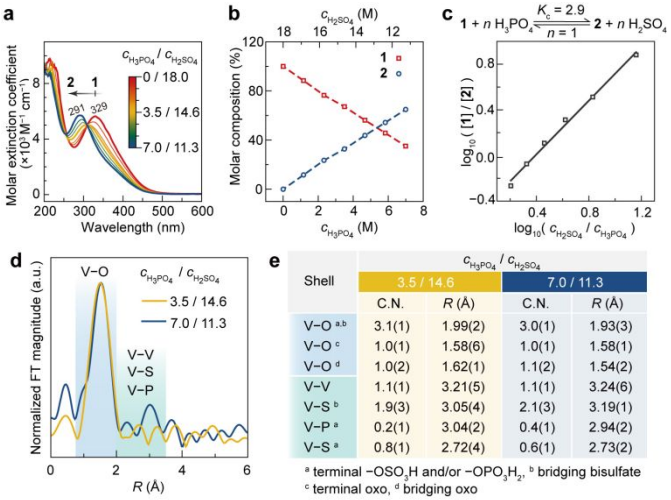

Fig. 2 a, UV-Vis spectra in different H_2SO_4-H_3PO_4 mixed solvents. C_V = 0.4 mM. **b**, the molar composition of **1** and **2** as a function of solvent composition. **c**, the logarithms of the concentration ratios between **1** and **2**, $\log_{10}([\mathbf{1}]/[\mathbf{2}])$, against the logarithms of the concentration ratios between H_2SO_4 and H_3PO_4, $\log_{10}(c_{H2SO4}/c_{H3PO4})$. **d**, **e**, EXAFS measurements (**d**) and structural optimization (**e**) for the vanadium(V)-oxo species in two representative electrolytes (c_{H3PO4}/c_{H2SO4} = 3.5/14.6 and 7.0/11.3). C_V = 10 mM.

perturbation to the electrocatalyst to study the role of the terminal $-OSO_3H$ ligand.

The activities of electrocatalytic CH_4 functionalization in H_3PO_4-H_2SO_4 mixed electrolyte were observed to decrease with the increase of c_{H3PO4}/c_{H2SO4} value hence the percentage of **2** in the solution. Representative cyclic voltammograms (CVs) in atmospheric N_2 (Fig. 3a and S3) and CH_4 (Fig. 3b and S4) of C_V = 10 mM were recorded at varying scan rates in H_3PO_4-H_2SO_4 electrolytes with 2 mm diameter Pt working electrode and all the following potentials are reported with respect to the Hg_2SO_4/Hg electrode. The vanadium V/IV redox couple was consistently at ~ 0.64 V. The generation of cation radical $V_2^{V,V\bullet+}$ via one-electron oxidation presumably from the terminal $-OSO_3H$ ligand (noted as **TLS** in Fig. 1a)[5c] was observed beyond 1.4 V. In general, the introduction of H_3PO_4 electrolyte suppresses or anodically shifts the oxidation current for the formation of cation radical and decreases the difference of oxidation current in N_2 and CH_4 atmosphere when electrode potential E > 1.4 V (Fig. 3a and 3b). Such observations reinforce our hypothesis that mono-substituting one redox-active terminal bisulfate in **1** with redox-inactive dihydrogen phosphate in **2** leads to a more oxidatively demanding electrogeneration of CH_4-reactive cation radical and a smaller electrocatalytic current density in the CH_4 environment. Our investigation continued with the experiments of bulk electrolysis under 1-bar CH_4 with C_V = 10 mM in H_3PO_4-H_2SO_4 electrolyte when E = 1.75 to 2.45 V with a FTO working electrode (Fig. S5). CH_3OSO_3H was the only product observed in the liquid phase (Fig. S6). The Faradaic efficiency (*FE*) and the partial current density of CH_4 oxidation to CH_3OSO_3H (j_{CH4}) were recorded in Fig. 3c and 3d. At small E values, CH_4 activation seemed to be kinetically controlled and increased with larger E until E > 2.25 V when other limiting factors including mass transport surfaced. While the optimal values of *FE* and j_{CH4} were all achieved at ca. 2.2 V, the electrolytes of larger c_{H3PO4}/c_{H2SO4} values in general lead to lower values of *FE* and j_{CH4}, consistent with the presumed lower redox activities incurred by dihydrogen phosphate substitution. More strikingly, Tafel analysis by plotting $\log_{10}(j_{CH4})$ versus E leads to different values of Tafel slopes in different H_3PO_4-H_2SO_4 mixtures. In Fig. 3e, when [**1**]/[**2**] ratios correspond to 100/0 and 67/33 (Table S1, c_{H3PO4}/c_{H2SO4} = 0/18.0 (red) and 3.5/14.6 (yellow), respectively), nearly overlapping data points were recorded when E < 2.1 V with Tafel slopes of 116 and 114 mV/dec, respectively. While their differences at E > 2.1 V may be indicative of the differences in [**1**]/[**2**] ratios, the similar if not the same Tafel slopes of about 120 mV/dec indicate the same turnover-limiting step (TLS) of electron transfer (*E* step),[14] which is presumed to be the first electrochemical oxidation of **1** into cation radical $V_2^{V,V\bullet+}$ with a redox-active terminal bisulfate ligand as reported before (step **TLS** in Fig. 1a).[5c] The same values of Tafel slopes at c_{H3PO4}/c_{H2SO4} = 0/18.0 and 3.5/14.6 also suggest that H_2SO_4 molecule does not participate in the TLS and the TLS is independent from the H_2SO_4 concentration. However, a Tafel slope of 188 mV/dec was observed (blue in Fig. 3e) when c_{H3PO4}/c_{H2SO4} = 7.0/11.3 and [**1**]/[**2**] ratio is 35/65 (Table S1). Such a Tafel slope much larger than 120 mV/dec indicates a TLS of chemical reaction (*C* step) preceding any electrochemical charge transfers.[14] This observation also excludes a possible shift of TLS to the step of CH_4 activation after the formation of $V_2^{V,V\bullet+}$, because a turnover-limiting chemical step of CH_4 activation (*C* step) in an *EC'* mechanism would have led to a smaller Tafel slope[14] that is not what we have observed experimentally. At high c_{H3PO4}/c_{H2SO4} values, a pre-equilibrium between **1** and **2** exists due to the predominance of **2** (Fig. 1b) and a *C* step converting **2** into **1** becomes turnover-limiting before the electrochemical oxidation of **1** into CH_4-reactive $V_2^{V,V\bullet+}$.

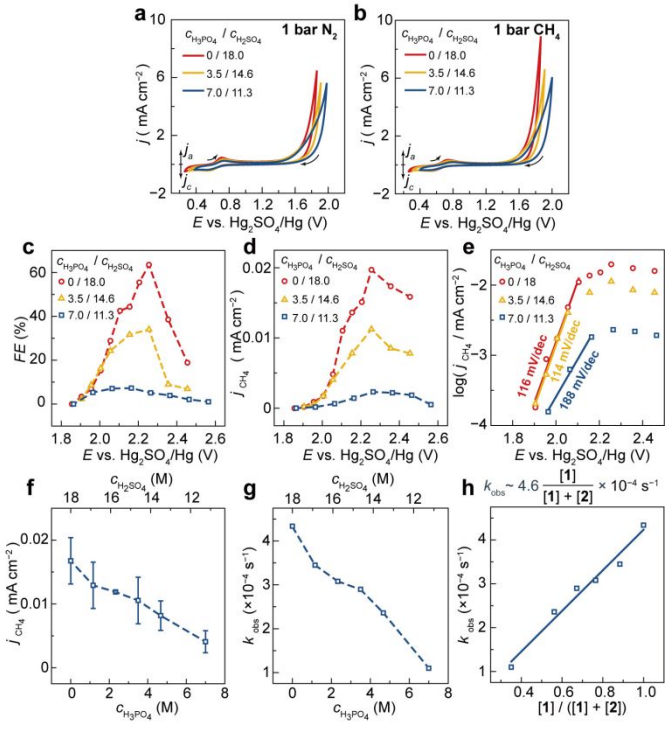

Fig. 3 **a**, **b**, CVs in 1-bar N_2 (**a**) and CH_4 (**b**). 100 mV/s. **c** to **e**, Faradaic efficiencies (**c**) and partial current densities (**d**) and the Tafel plots (**e**) measured at different potentials. **f** to **h**, partitioning the reactivities between **1** and its dihydrogen-phosphate-substituted variant **2**, E = 2.25 V. **f**, **g**, partial current densities (**f**) and apparent rate constants (**g**) as a function of the composition in H_3PO_4-H_2SO_4 mixed electrolyte. **h**, The relationship between apparent rate constants and molar composition of **1**. Each data point shows the average of three individual measurements. C_V = 10 mM.

The analysis of the pseudo-first-order apparent rate constant k_{obs} of CH_4 electrocatalysis at different values of c_{H3PO4}/c_{H2SO4} support the hypothesized redox inactivity of **2** and that only **1** is directly electrochemically oxidizable to yield CH_4-reactive cation radical $V_2^{V,V\bullet+}$. At E = 2.25 V, j_{CH4} was obtained at different values of c_{H3PO4}/c_{H2SO4} (Fig. 3f). The average values of k_{obs} based on C_V were determined from the diffusion coefficient of vanadium(V)-oxo dimer at different values of c_{H3PO4}/c_{H2SO4} (Fig. S7, Table S3, ESI†).[15] Fig. 3g depicts k_{obs} as a function of c_{H3PO4} and c_{H2SO4} in the electrolyte. In Fig. 3f and 3g, the average activities of CH_4 activation decrease with increasing c_{H3PO4} under the same C_V. The 4.3-fold and 3.9-fold changes of j_{CH4} (Fig. 3f) and k_{obs} (Fig. 3g), respectively, under a 1.6-fold decrease of c_{H2SO4} suggest that the observed changes of j_{CH4} and k_{obs} do not directly originate from the change of the TLS's kinetic rate that might have been a function of c_{H2SO4}, because the Tafel slope analysis suggests that H_2SO_4 molecule does not participate in the turnover-limiting one-electron oxidation of $V_2^{V,V}$. We further plotted k_{obs} as a function of the percentage of **1** in the mixture of **1** and **2**, [**1**]/([**1**]+[**2**]), under different values of

c_{H3PO4}/c_{H2SO4} at C_V = 10 mM (Fig. 3h). A linear relationship was observed and extrapolation of this linear relationship yields k_{obs} = (4.2 ± 0.5)×10^{-4} and (−0.4 ± 0.3)×10^{-4} s^{-1} when [**1**]/([**1**]+[**2**]) = 1.0 (pure **1**) and 0.0 (pure **2**), respectively. The significant difference of calculated k_{obs} between **1** and **2** quantitatively confirms that only **1** is electrochemically oxidizable to a CH_4-reactive cation radical and **2** is redox-innocent at E = 2.25 V. It is intriguing that replacing only one of the two terminal $-OSO_3H$ moieties in **1** with $-OPO_3H_2$ leads to such a dramatic difference of k_{obs} between **1** and **2**. Although the electrochemically generated cation radical $V_2^{V,V\bullet+}$ is computationally considered as a radical localized on the terminal oxygen atom of the monodentate bisulfate ligand (Fig. 1a),[5c] our results hint that the singly occupied molecular orbital (SOMO) of $V_2^{V,V\bullet+}$ is highly delocalized across the whole vanadium(V)-oxo dimer. A $-OPO_3H_2$ moiety away from the formally electrooxidized $-OSO_3H$ moiety has a significant impact on the energetics of the electrogenerated cation radical. Such results are indeed supportive of the computational results in the study of electrochemically generated $Pd_2^{III,III}$ dimer in H_2SO_4.[8] Thanks to the covalent nature of the Pd−O bond and the possible formation of delocalized biradical, two equally viable CH_4-activation pathways were proposed for the $Pd_2^{III,III}$ dimer and both include the step of H-atom abstraction from CH_4 initiated by an O atom in the metal-bound bisulfate ligand (Fig. S1).[8] In our work, because the pre-catalyst $V_2^{V,V}$ **1** has already been at vanadium's highest formal oxidation state that precludes any metal-based oxidation and metalloradical formation, our experiments provide clean evidence that bisulfate is redox-active during electrocatalytic CH_4 activation. Given the similar electrochemical driving forces between the vanadium-based electrocatalysis and others,[5a, 5b, 16] one working hypothesis is that the redox noninnocence of metal-bound bisulfate is universally present in electrocatalytic CH_4 activation in H_2SO_4-based electrolyte. Indeed, the universal reactivities of electrocatalytic CH_4 functionalization across early transition metals (Group 4 to 6, Period 4 to 6) reported by our group recently offer additional support towards our argument.[16] While we do not have enough information to extend such hypothesis for homogenous CH_4 functionalization in H_2SO_4 or oleum through electrophilic activation,[7a-d] we contend that the redox activity of metal-bound bisulfate should be considered during mechanistic investigation.

Our results offer a reminder in the context of translating electrocatalysis of CH_4 activation in currently prevailing yet unfriendly H_2SO_4 solvent[17] to a more benign electrolyte. The removal of H_2SO_4 solvent not only destabilizes CH_3OH or its equivalent as the two-electron oxidation product,[6] but also may inadvertently remove the electrocatalytic active species important towards activating CH_4 and alter the overall reaction mechanism. Designing a bisulfate-rich microenvironment for the electrocatalytic active sites with minimal H_2SO_4 usage could be a possible route to keep the electrocatalytic mechanism and activity of CH_4 functionalization with least infrastructure reliance and environmental footprints.

H.M.C. acknowledges the Ministry of Science and Technology, Taiwan (Contract no. MOST 107-2628-M-002015-RSP). C.L. acknowledges the NSF Award (CHE-1955836), and the startup fund from the University of California, Los Angeles.

There are no conflicts to declare.

Notes and references

1. (*a*) E. J. Dlugokencky and P. Bousquet, *Science*, 2014, **343**, 493-495. (*b*) D. Malakoff, *Science*, 2014, **344**, 1464-1467. (*c*) N. J. Gunsalus, A. Koppaka, S. H. Park, S. M. Bischof, B. G. Hashiguchi and R. A. Periana, *Chem. Rev.*, 2017, **117**, 8521-8573. (*d*) O. Edenhofer, et. al., *Working Group III Contribution to the Fifth Assessment Report of the Intergovernmental Panel on Climate Change, Climate Change 2014: Mitigation of Climate Change*, Cambridge University Press, 2015.
2. J. Rostrup-Nielsen and L. J. Christiansen, *Concepts in Syngas Manufacture*, Imperial College Press, 2011.
3. (*a*) M. Ravi, M. Ranocchiari and J. A. van Bokhoven, *Angew. Chem. Int. Ed.*, 2017, **56**, 16464-16483. (*b*) X. Meng, X. Cui, N. P. Rajan, L. Yu, D. Deng and X. Bao, *Chem*, 2019, **5**, 2296-2325.
4. (*a*) R. A. Periana, D. J. Taube, S. Gamble, H. Taube, T. Satoh and H. Fujii, *Science*, 1998, **280**, 560-564. (*b*) R. A. Periana, et. al., *Science*, 1993, **259**, 340-343. (*c*) N. Basickes, T. E. Hogan and A. Sen, *J. Am. Chem. Soc.*, 1996, **118**, 13111-13112.
5. (*a*) M. E. O'Reilly, R. S. Kim, S. Oh and Y. Surendranath, *ACS Cent. Sci.*, 2017, **3**, 1174-1179. (*b*) D. Xiang, J. A. Iñiguez, J. Deng, X. Guan, A. Martinez and C. Liu, *Angew. Chem. Int. Ed.*, 2021, **60**, 18152-18161. (*c*) J. Deng, et. al., *Nat. Commun.*, 2020, **11**, 3686.
6. M. Ahlquist, R. J. Nielsen, R. A. Periana and W. A. Goddard III, *J. Am. Chem. Soc.*, 2009, **131**, 17110-17115.
7. (*a*) C. J. Jones, D. Taube, V. R. Ziatdinov, R. A. Periana, R. J. Nielsen, J. Oxgaard and W. A. Goddard III, *Angew. Chem. Int. Ed.*, 2004, 43, 4626-4629. (*b*) J. T. Fuller, S. Butler, D. Devarajan, A. Jacobs, B. G. Hashiguchi, M. M. Konnick, W. A. Goddard, J. Gonzales, R. A. Periana and D. H. Ess, *ACS Catal.*, 2016, 6, 4312-4322. (*c*) T. R. Cundari, L. A. Snyder and A. Yoshikawa, *J. Mol. Struct.(Theochem)*, 1998, **425**, 13-24. (*d*) S. Chempath and A. T. Bell, *J. Am. Chem. Soc.*, 2006, **128**, 4650-4657. (*e*) S.-S. Chen, A. Koppaka, R. A. Periana and D. H. Ess, *J. Am. Chem. Soc.*, 2021, **143**, 18242-18250.
8. R. S. Kim, A. Nazemi, T. R. Cundari and Y. Surendranath, *ACS Catal.*, 2020, **10**, 14782-14792.
9. (*a*) H. Jakob, S. Leininger, T. Lehmann, S. Jacobi and S. Gutewort, in *Ullmann's Encyclopedia of Industrial Chemistry*, Wiley-VCH, Weinheim, 2012, vol. 26, pg. 293. (*b*) K. Groenen Serrano, *Curr. Opin. Electrochem.*, 2021, **27**, 100679.
10. C. Madic, G. M. Begun, R. L. Hahn, J. P. Launay and W. E. Thiessen, *Inorg. Chem.*, 1984, **23**, 469-476.
11. (*a*) A. B. P. Lever, *J. Chem. Educ.*, 1974, **51**, 612. (*b*) R. L. DeKock and H. B. Gray, *Chemical Structure and Bonding*, University Science Books, Mill Valley, California, 2nd edn., 1989.
12. G. L. Miessler, P. J. Fischer and D. A. Tarr, *Inorganic Chemistry*, Pearson Education, Inc, New York, 5th edn., 2014.
13. (*a*) S. E. Braslavsky, *Pure Appl. Chem.*, 2007, **79**, 293-465. (*b*) M. D. Cohen and E. Fischer, *J. Chem. Soc.*, 1962, 3044-3052.
14. J. B. Allen and R. F. Larry, *Electrochemical Methods: Fundamentals and Applications*, John Wiley & Sons, 2nd edn., 2001.
15. P. Zanello, C. Nervi and F. F. de Biani, *Inorganic Electrochemistry: Theory, Practice and Application*, RSC, Cambridge, UK, 2003.
16. J. Deng, et. al., *Angew. Chem. Int. Ed.*, 2021, **60**, DOI:10.1002/anie.202107720.
17. G. Busca, *Chem. Rev.*, 2007, **107**, 5366-5410.

